Electron–electron scattering rate in presence of random impurity potential in low-dimensional systems



2004 J. Phys.: Condens. Matter 16 3117

(http://iopscience.iop.org/0953-8984/16/18/013)

INSTITUTE OF PHYSICS PUBLISHING JOURNAL OF PHYSICS: CONDENSED MATTER

J. Phys.: Condens. Matter **16** (2004) 3117–3132 PII: S0953-8984(04)70178-2

# Electron–electron scattering rate in presence of random impurity potential in low-dimensional systems

**A C Sharma and S S Z Ashraf**

Physics Department, Faculty of Science, MS University of Baroda, Vadodara-390002, India

Received 9 October 2003
Published 23 April 2004
Online at stacks.iop.org/JPhysCM/16/3117
DOI: 10.1088/0953-8984/16/18/013

**Abstract**

The electron–electron scattering rate ($1/\tau_{ee}$) in the presence of a random disorder potential has been computed, within the random phase approximation, as a function of excitation energy ($\varepsilon$) for a quantum well (QWL), a quantum wire (QWR) and a periodic quantum wire structure (QWS). It is found that: (i) $1/\tau_{ee}$ goes to zero when $\varepsilon \to 0$ and (ii) the $\varepsilon$ dependence as well as the magnitude of $1/\tau_{ee}$ are determined by the value of the inverse electron–impurity collision time ($1/\tau$), the carrier density and the width of a QWR. The computed $1/\tau_{ee}$ exhibits its maximum value for $1/\tau \to 0$ and it decreases thereafter on increasing $1/\tau$, for all values of $\varepsilon$ and other parameters. The computed $1/\tau_{ee}$ of a QWR declines monotonically with the width of the QWR and it reduces to $1/\tau_{ee}$ of a QWL at larger wire widths, for a given value of $\varepsilon$ and the other intrinsic parameters. The $1/\tau_{ee}$ of a QWS differs from that of a QWR because of the added contribution from inter-wire electron–electron interactions in a QWS. For the given values of $\varepsilon$, $1/\tau$, carrier density and the width of a QWR, the $1/\tau_{ee}$ of a QWS is found to be smaller than that of a QWR and larger than that of a QWL. This suggests that the electron–electron scattering rate is enhanced on the reduction in the effective dimensionality of a system. Our theoretical study of $1/\tau_{ee}$ and its dependence on various intrinsic parameters of QWL, QWR and QWS suggests, in conclusion, that a quasi-particle Fermi liquid description can be applied to electron–electron scattering in the presence of an electron-disorder potential scattering, at zero temperature, in low-dimensional systems.

## 1. Introduction

The many-body theoretical description of a system of electrons involves an important concept of quasi-particle lifetime. The life of an electron in a given state is determined by the scattering rate that is largely contributed by electron–electron scattering in an interacting electron system. The quasi-particle description of electrons in an interacting system (degenerate fermions) is based on the assumption that the inverse lifetime of an electronic excitation is small compared to its excitation energy ($\varepsilon$) above Fermi level. As a consequence, the electronic distribution

  

function in a degenerate Fermi system shows a sharp discontinuity at the Fermi level. These assertions are mainly based on the assumption that in quasi-particle scattering only large and energy-independent momentum transfers are essential, which is basically true for bulk phenomena. However, a quasi-particle description may break down in one-dimensional (1D) and quasi-1D systems when a strong electron–electron interaction results in a rapid decay of electronic excitations. There has been a widely held viewpoint that the scattering of electrons by a random impurity (disorder) potential could restore the Fermi surface and a Fermi-liquid quasi-particle description can be applied to these systems. The electron scattering from a disorder potential is unavoidable, since a small amount of residual impurities always exists in a realistic low-dimensional system, doped/modulation doped semiconductor structure. The disorder effects are specific to a confined system that exhibits the strong deviations from bulk behaviour, depending on the ratio of system size and disorder correlation length. It is to answer these questions that we performed a theoretical study of the inelastic scattering rate for electron–electron scattering, $1/\tau_{ee}$, in the presence of a disorder potential in a quantum well (QWL), a quantum wire (QWR) and a periodic structure of quantum wires (QWS). Another aim of this paper is to see whether or not a satisfactory description of electron–electron scattering in 1D and quasi-1D systems consisting of a significant randomized disorder potential can be provided beyond the Tomonaga–Luttinger model. The Tomonaga–Luttinger model makes some drastic simplifying assumptions that make the comparison between model calculations and the experimental results somewhat tenuous.

Apart from the construction of a many-body theory, the decay time of an electronic excitation plays an important role in a number of physical processes, such as damping of collective excitations, dephasing of localized electrons, optical transitions, Hall effect, etc. The electron–electron scattering rate in the presence of a disorder potential leads to the quantum corrections to: (i) the conductivity and its nontrivial temperature dependence and (ii) thermodynamical quantities of the electron gas. The physical relaxation process of an electron is inelastic and its characteristics timescale depends on the details of those scatterings that give rise to real transitions. In addition to the scattering rate, the momentum relaxation rate and the energy relaxation rate are also defined. The momentum relaxation rate determines the current whereas the energy relaxation rate is related to the average energy of an electron in the presence of fields. The relative importance of these three rates is decided by the property we are interested in, for a given system.

There have been large numbers of theoretical and experimental studies on electron–electron scattering and related aspects of a two-dimensional electron gas (2DEG) [1–6] and one-dimensional electron gas (1DEG) [7–12] in the presence of a random impurity potential. Disorder caused by impurities has important consequences in the many-body properties of low-dimensional electron systems. Several good review articles exist in the field [13, 14]. Some of the recent publications in this field deal with electron–electron scattering in heterostructures and superlattice structures [3, 15], the effects of electron–electron scattering on electron beam propagation in a 2DEG [16], relaxation of excited electrons in a paramagnetic electron gas [17], electron–electron scattering in low diffusivity thick $RuO_2$ and $IrO_2$ films [18], electron–electron scattering and linear transport in two-dimensional systems [19], transport properties of a quantum wire in the presence of impurities and long range Coulomb force [20], electron–electron scattering in quantum wires and the spin effects [21], intrasubband and intersubband inelastic scattering rates due to electron–electron interactions in quantum wire structures [22] and the relative importance of electron–electron interactions and disorder in 2D metallic state [23].

In this paper, we present a calculation of $1/\tau_{ee}$ as a function of $\varepsilon$ and the electron–impurity collision time ($\tau$), within the random phase approximation (RPA), for a QWL, QWR and

QWS, which are referred to as $1/\tau_{ee}^{1}(\varepsilon,\tau)$, $1/\tau_{ee}^{2}(\varepsilon,\tau)$ and $1/\tau_{ee}^{3}(\varepsilon,\tau)$, respectively. Our calculations are performed for the momentum transfer, $q$, and frequency, $\omega$, space that has the correct diffusive behaviour and belongs to the phase space around the Fermi surface. The earlier studies on electron–electron scattering in the presence of a random disorder potential in 2DEG and 1DEG have been performed for $q$ and $\omega$ not covering the entire diffusive behaviour regime. Our computed $1/\tau_{ee}^{2}(\varepsilon,\tau)$ and $1/\tau_{ee}^{1}(\varepsilon,\tau)$ significantly differ both in magnitude as well as in behaviour from their previously reported values [24]. Our calculations are applicable to short range disorder systems such as doped homo-junctions, where a doped impurity coexists with conduction electrons, and the modulation doped hetero-junctions consisting of spatially separated impurities and conduction electrons. The spatially separated impurities yield a relatively smooth disorder potential. The paper is divided into four sections. The formalism is described in section 2. Calculations and the discussion of the results for QWL, QWR and QWS are given in sections 3–5, and finally our work is summarized in section 6.

## 2. Formalism

We consider the case of a degenerate electron gas, in the presence of a randomized disorder potential confined to a QWL, QWR and QWS, at a temperature $T = 0$. Our calculation is basically performed within RPA with simplifying assumptions that the Fermi energy and other energy scales pertinent to the system are small compared to the energy separation between the lowest energy subband and the higher energy subbands. We further assume that a spatially randomized potential is distributed according to the Gauss-$\delta$ correlation law. The products of pair correlators can represent all the correlators and the Born approximation can be used for the interactions with short range impurities [25]. In order to keep our treatment simple, we avoid microscopic models that treat the realistic distribution of randomized impurities [26]. A simple treatment of disorder effects in nanostructures is given by Richer [25]. The inverse electron–impurity time, $1/\tau$, can be given by: $1/\tau = \pi\upsilon\nu\langle U^2\rangle$, where $\nu$ is the density of states and $\langle U^2\rangle = c_{im}(\int v(r)\,\mathrm{d}r)^2$. $C_{im}$ is the impurity concentration and $v(r)$ is the single impurity potential [24]. $1/\tau$ is independent of momentum and energy. Our calculations are performed for intrasubband transitions within the ground subband. The RPA $1/\tau_{ee}$ in the presence of a disorder potential is given by [24]

$$\frac{1}{\tau_{ee}(\varepsilon)} = \frac{8}{\pi^3\nu}\sum_{q}\sum_{q_1}\int_0^{\varepsilon}\mathrm{d}\omega\int_{-\omega}^{0}\mathrm{d}\varepsilon' V(\omega,\boldsymbol{q})V^*(\boldsymbol{q}_1,\omega) \times \prod(\varepsilon,\varepsilon-\omega,\boldsymbol{q},\boldsymbol{q}_1)\prod(\varepsilon',\varepsilon'+\omega,\boldsymbol{q},\boldsymbol{q}_1). \tag{1}$$

The screened electron–electron interaction, $V(\boldsymbol{q},\omega)$, is defined as

$$V(\boldsymbol{q},\omega) = \frac{V^0(\boldsymbol{q})}{1+V^0(\boldsymbol{q})\pi(\boldsymbol{q},\omega)} \tag{2}$$

where, $V^0(\boldsymbol{q})$ is the bare Coulomb potential and $\pi(\boldsymbol{q},\omega)$ is the electronic polarization function. To obtain the response function, $\prod(\varepsilon,\varepsilon-\omega,\boldsymbol{q},\boldsymbol{q}_1)$ averaging over the impurity configuration is done by separating the contribution to $1/\tau_{ee}$ from the diffusion poles, which correspond to a change in the interaction time due to diffusion and are related to a singularity in the particle–hole channel. The impurity potential used in averaging is shown in figure 1(a). The full lines represent the bare Green function and the broken lines correspond to random potential correlators. After averaging, the $\prod(\varepsilon,\varepsilon-\omega,\boldsymbol{q},\boldsymbol{q}_1)$ is given by [24]

$$\prod(\varepsilon,\varepsilon-\omega,\boldsymbol{q},\boldsymbol{q}_1) = \frac{\pi\nu\tau}{2}\delta_{qq_1}\,\mathrm{Re}[\xi(\varepsilon,\boldsymbol{q},\omega)D(\varepsilon,\boldsymbol{q},\omega) - \xi'(\varepsilon,\boldsymbol{q},\omega)D'(\varepsilon,\boldsymbol{q},\omega)]. \tag{3}$$

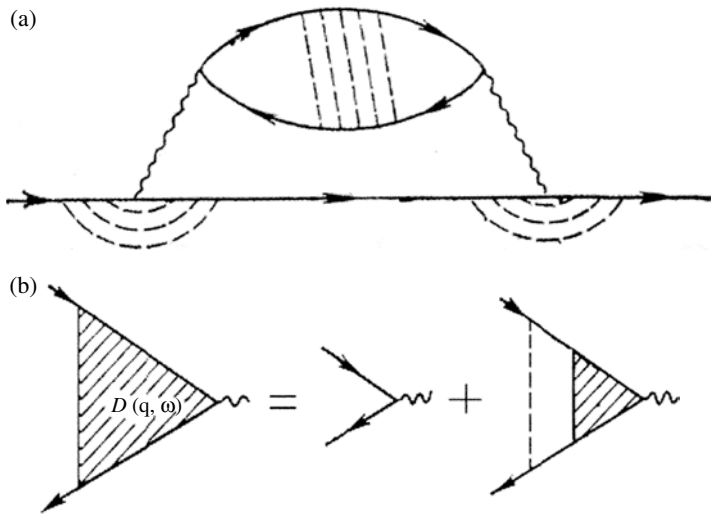


**Figure 1.** (a) Impurity configuration potential diagram and (b) the ladder diagrams. Full lines correspond to bare Green functions and broken lines correspond to random potential correlators.

The $D(\varepsilon, \boldsymbol{q}, \omega)$ is the sum of the ladder diagrams as is shown in figure 1(b). The $D'(\varepsilon, \boldsymbol{q}, \omega)$ differs from $D(\varepsilon, \boldsymbol{q}, \omega)$ in complex conjugation for all Green functions with energy, $\varepsilon - \omega$. On solving the equation depicted in figure 1(b), one gets [24]

$$D(\varepsilon, \boldsymbol{q}, \omega) = \frac{1}{1 - \xi(\varepsilon, q, \omega)} \tag{4}$$

$$D'(\varepsilon, \boldsymbol{q}, \omega) = \frac{1}{1 - \xi'(\varepsilon, q, \omega)} \tag{5}$$

where

$$\xi(\varepsilon, \boldsymbol{q}, \omega) = \frac{1}{\pi \nu \tau} \int (\mathrm{d}p) G(\varepsilon, \boldsymbol{p}) G(\varepsilon - \omega, \boldsymbol{p} - \boldsymbol{q}), \tag{6}$$

$$\xi'(\varepsilon, \boldsymbol{q}, \omega) = \frac{1}{\pi \nu \tau} \int (\mathrm{d}p) G(\varepsilon, \boldsymbol{p}) G^*(\varepsilon - \omega, \boldsymbol{p} - \boldsymbol{q}). \tag{7}$$

In equation (3), $\delta_{qq_1}$ is the Kronecker delta function and Re stands for the real part of the quantity in brackets. $G(\varepsilon, \boldsymbol{p})$ is the electron Green function averaged over the impurity configuration shown in figure 1(a). Due to the analytical properties of $G(\varepsilon, \boldsymbol{p})$, the $\xi(\varepsilon, \boldsymbol{q}, \omega)$ is small in parameter $(\hbar/\tau\varepsilon_{\mathrm{F}})$ when $\varepsilon$ and $\varepsilon - \omega$ have the same signs, where $\varepsilon_{\mathrm{F}}$ is the Fermi energy. Therefore

$$\xi(\varepsilon, \boldsymbol{q}, \omega) = \xi(\boldsymbol{q}, \omega)[\theta(\varepsilon)\theta(\omega - \varepsilon) + \theta(-\varepsilon)\theta(\varepsilon - \omega)] \tag{8}$$

$$\xi'(\varepsilon, \boldsymbol{q}, \omega) = \xi(\boldsymbol{q}, \omega)[\theta(\varepsilon)\theta(\varepsilon - \omega) + \theta(-\varepsilon)\theta(\omega - \varepsilon)]. \tag{9}$$

Then for $\omega < \varepsilon$, the $\prod(\varepsilon, \varepsilon - \omega, \boldsymbol{q}_1)$, for $\omega < \varepsilon$ can be simplified to

$$\prod(\varepsilon, \varepsilon - \omega, \boldsymbol{q}, \boldsymbol{q}_1) = \frac{\pi \nu \tau}{2} \delta_{qq_1} \,\mathrm{Re}\left[\frac{\xi(q, \omega)}{1 - \xi(q, \omega)}\right]. \tag{10}$$

This results in

$$\frac{1}{\tau_{\mathrm{ee}}(\varepsilon, \tau)} = \frac{2}{\pi \nu} \int_0^{\varepsilon} \omega \,\mathrm{d}\omega \int \frac{\mathrm{d}\vec{\boldsymbol{q}}}{(2\pi)^d} |V(\omega, \boldsymbol{q})|^2 \left[\mathrm{Re}\left\{\frac{\nu\tau\xi(\boldsymbol{q}, \omega)}{1 - \xi(\boldsymbol{q}, \omega)}\right\}\right]^2 \tag{11}$$

where $d$ takes the value 3, 2 and 1 for 3D, 2D and 1D systems, respectively. Equation (11) is applicable to the case of an arbitrary dimensionality. The evaluation of $\nu$, $V(\boldsymbol{q}, \omega)$ and $\xi(\boldsymbol{q}, \omega)$ for a given system depend on its dimensionality. Equations (1)–(11) are obtained by treating $\tau$ independent of energy and momentum. The major contributions to $1/\tau_{ee}(\varepsilon, \tau)$, when $\varepsilon \leqslant \varepsilon_F$, come from virtual single-particle transitions in the case of 2D systems and from virtual plasmons in the case of 1D systems [8].

## 3. A quantum well (2D electron gas system)

A quantum well consists of a number of energy subbands. The single-particle transitions that predominantly contribute to $1/\tau_{ee}$ for $\varepsilon$ smaller than the intersubband energy separation between the ground subband and higher subbands are the intrasubband transitions within the ground subband. Evaluation of $\nu$ and $\prod(\boldsymbol{q}, \omega)$ for $q$ and $\omega$ confined to single-particle excitations, $q \leqslant 2k_F$ and $|\omega + i/\tau| \leqslant q v_F$, gives [24]

$$\nu_1 = \frac{2m_e^*}{\pi\hbar^2}, \tag{12a}$$

$$V_1(\boldsymbol{q}, \omega) = \frac{2\pi e^2}{\varepsilon_0} \frac{1}{\left[\boldsymbol{q} + \frac{g_0 D_1 q^2}{-i\omega + D_1 q^2}\right]}. \tag{12b}$$

where $m_e^*$ is the effective mass of an electron. Evaluation of equation (6) along with (8) gives [24]

$$\xi_1(\boldsymbol{q}, \omega) = \frac{1}{\sqrt{(1 - i\omega\tau)^2 + q^2 l^2}}. \tag{13}$$

Subscript (superscript) 1 stands for a QWL. The 2D diffusion coefficient, $D_1 = v_F^2\tau/2$, and mean free path $l = v_F\tau$. $v_F$ is the Fermi velocity and $k_F$ is the Fermi wavevector. $\varepsilon_0$ is the background dielectric constant and the inverse screening length, $g_0 = 4m_e^* e^2/\varepsilon_0\hbar^2$. Equation (8) for a QWL can be rewritten in terms of dimensionless quantities as follows:

$$\frac{\hbar}{\tau_{ee}^1(x, S)\varepsilon_F} = \frac{K^2}{\pi} \int_0^x y\,dy \int_{z_0}^2 dz\, \frac{(4z^4 + y^2S^2)}{z[4(z+K)^2z^2 + y^2S^2]} \left[\mathrm{Re}\left\{\frac{1}{S - \sqrt{(S - iy)^2 + 4z^2}}\right\}\right]^2, \tag{14}$$

where $S = \hbar/\tau\varepsilon_F$ is the normalized broadening, $x = \varepsilon/\varepsilon_F$ is the normalized energy, $K = g_0/k_F$ is the normalized inverse screening length, $z = q/k_F$ and $y = \hbar\omega/\varepsilon_F$.

Equation (14) is applicable to weak as well as strong disorder potential cases. An analytical solution of equation (14) for all values of $x$ and $S$ is not possible. The analytical solutions that are valid for limited values of $x$ and $S$ can be obtained, however. We performed the $z$ and $y$ integrations for $S \ll 1$ (close to zero) to obtain

$$\begin{aligned}\frac{\hbar}{\tau_{ee}^1(x, S)\varepsilon_F} = \frac{K^2}{2\pi}\Bigg[ & I_0\left\{2\ln(4/S) - 12K^2 + 2K + K^3/3 - 2\ln(2+K) - \frac{2K}{2+K}\right\} \\ & + 2J_0\{1 - \ln(2x/S)\} + K_0\left\{\ln(K + \alpha/2) + \frac{4K(K+\alpha)}{\alpha(\alpha+2K)}\right\} + \frac{4K(K-\alpha)}{\alpha(\alpha-2K)}L_0 \\ & + \frac{1}{(1-r^2)}\Bigg\{4r^2\ln(2+K) + 2\ln(K + x_0/2) - 4r^2(2K^2 - \ln(4/S)) \\ & + 2r\left(2\ln(S/2x) + Kr + \frac{K^3 r}{12}\right)\Bigg\} + \frac{1}{2}\ln(x_0 + \alpha)\ln\left(\frac{x_0 + \alpha}{4}\right)\end{aligned}$$

$$-\frac{1}{2}\ln(S+\alpha)\ln\left(\frac{S+\alpha}{4}\right)+\sum_{m=1}^{\infty}\frac{(-1)^{m+1}}{m^2}\left\{\left(\frac{x_0-\alpha}{\alpha+2K}\right)^m-\left(\frac{S-\alpha}{\alpha+2K}\right)^m\right\}$$
$$+\frac{Kx^2}{24}-4K^2r^2-2\ln(K+S/2)-2\{1-\ln(S^2/2)\}\ln\left(\frac{1-t}{1+t}\right)$$
$$+2\frac{2t}{(1-t^2)}\ln(2)-\frac{2}{K}\{(x-S)+(x^3-S^3)/36K^2+(x^5-S^5)/400K^4\}\Bigg] \tag{15}$$

where

$$x_0=\sqrt{x^2+S^2},\qquad \alpha=\sqrt{4K^2+S^2},\qquad I_0=\ln(1-r^2),$$
$$J_0=\ln\left(\frac{1-r}{1+r}\right),\qquad K_0=\ln\left(\frac{\alpha-x_0}{\alpha-S}\right),\qquad L_0=\ln\left(\frac{\alpha+x_0}{\alpha+S}\right),$$
$$r=x/2\,\mathrm{K}\qquad\text{and}\qquad t=S/2\,\mathrm{K}.$$

The analytical results for $1/\tau_{ee}^{1}(\varepsilon)$ in the absence of a disorder potential ($S=0$) has also been reported [3]. However, these results were obtained by taking $z \ll K$ and $y \ll 2z$, in terms of our notation. The approach was justified by arguing that only $z$ values close to $z_0$ and $y$ values close to zero make the most dominant contributions to $1/\tau_{ee}^{1}(x, S)$. Our calculated reduced electron–electron scattering rate, given by equation (15), is therefore more accurate compared to that reported by Riezer and Wilkins [3] and it is applicable to the weak disorder potential case instead of the zero disorder potential case. Following the argument of Riezer and Wilkins, equation (14) can be simplified to

$$\frac{\hbar}{\tau_{ee}^{1}(x,s)\varepsilon_F}=\frac{1}{\pi}\int_0^x y\,\mathrm{d}y\int_{z_0}^{K}\frac{z\,\mathrm{d}z}{(4z^2+S^2-y^2)^2} \tag{16}$$

whose validity is better for the case of $S \ll 1$ and $x \ll 1$. On performing $z$ and $y$ integrations, we obtain

$$\frac{\hbar}{\tau_{ee}^{1}(x,S)\varepsilon_F}=\frac{1}{16\pi}\left[(4K^2+S^2)\ln\left(\frac{4K^2+S^2}{4K^2+S^2-x^2}\right)+x^2\ln\left(\frac{4K^2+S^2-x^2}{2S^2}\right)-x^2\right]. \tag{17}$$

In order to see how $1/\tau_{ee}(x, S)$ depends on the normalized energy and normalized broadening, which covers the weak as well as the strong disorder potential case, we numerically computed equation (14) for a GaAs quantum well having $m_e^* = 0.068\ m_e$ and $\varepsilon_0 = 12.5$ [28]. The $1/\tau_{ee}^{1}(x, S)$ first has been computed as a function $x$ for given $S$ and then as a function of $S$ for given $x$ at $k_F = 3.45\times10^6\ \mathrm{cm}^{-1}$ and $\varepsilon_F = 35.25$ meV. Our numerically computed $1/\tau_{ee}^{1}(x, S)$ from equations (14), (15) and (17) is plotted as a function of $x$ in figure 2 for two values of normalized broadening (0.001, 0.1). As can be seen from the figure, the simple analytical result, given by equation (17), gives very good agreement with detailed numerical results for $x < 0.5$ and $S \ll 1$. It is to be noted that equation (15) is an exact solution of equation (14), for $S \to 0$. We found that the computed $1/\tau_{ee}^{1}(x, S)$ as a function of $x$ can almost be fitted to a polynomial of type: $1/\tau_{ee}^{1}(x, S) = ax + bx^2 + cx^3$, for $0 \leqslant x \leqslant 1$. The coefficients $a, b$ and $c$ depend on $S$ and $k_F$. This has been found in agreement with experimentally measured conductivity, as a function of frequency, for a semiconductor inversion layer with disorder [27]. The $x$ dependence of our numerically computed $1/\tau_{ee}^{1}(x, S)$ differs from that shown by prior performed calculations for weak disorder potential case [2–5] as well as for the strong disorder potential case [24], where the proper $q$ and $\omega$ dependence of $V_1$ and $\xi_1$ was ignored.

Our numerically computed $1/\tau_{ee}^{1}(x, S)$ from equation (14), along with that from equations (15) and (17), is plotted in figure 3 as a function of $S$ for three values of normalized

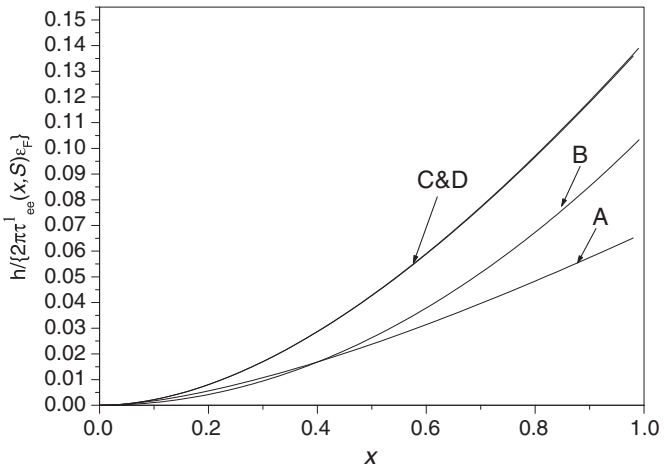


**Figure 2.** Dimensionless electron–electron scattering rate as a function of normalized energy for a quantum well at $k_F = 3.45 \times 10^6$ cm$^{-1}$, $\varepsilon_0 = 12.5$ and $\varepsilon_F = 35.25$ meV. Numerically computed results are from equation (14): curve A, when $\hbar/\tau\varepsilon_F = 0.1$ and curve C, for $\hbar/\tau\varepsilon_F = 0.001$. Analytical results: curve B using equation (17) at $\hbar/\tau\varepsilon_F = 0.1$ and curve D, using equation (15) for $\hbar/\tau\varepsilon_F = 0.001$.

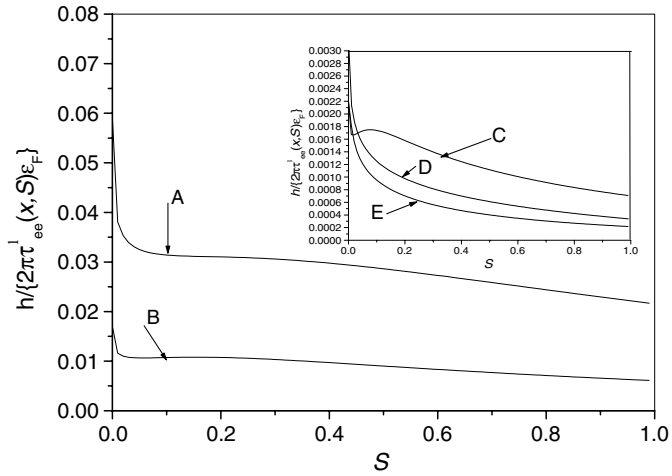


**Figure 3.** Dimensionless electron–electron scattering rate as a function of normalized broadening for a quantum well, at $k_F = 3.45 \times 10^6$ cm$^{-1}$, $\varepsilon_0 = 12.5$ and $\varepsilon_F = 35.25$ meV. Numerically computed results from equation (14): curve A, when $\varepsilon/\varepsilon_F = 0.6$; curve B, for $\varepsilon/\varepsilon_F = 0.3$ and curve C, when $\varepsilon/\varepsilon_F = 0.1$. Analytical results: curve D, using equation (15) at $\varepsilon/\varepsilon_F = 0.1$ and curve E, using equation (17) for $\varepsilon/\varepsilon_F = 0.1$.

energy (0.1, 0.3, 0.6), $k_F = 3.45 \times 10^6$ cm$^{-1}$ and $\varepsilon_F = 35.25$ meV. The $1/\tau^1_{ee}(x, S)$ shows rapid decline with $S$ when $0 < S < 0.1$, as is seen from the figure. This suggests that the electron scattering rate exhibits a stronger dependence on the disorder potential for a dilute impurity distribution. Figure 3 also shows that the overall agreement between our analytical results and the detailed numerical results is good, which justifies our approximations employed in obtaining simple analytical results. We also computed $1/\tau^1_{ee}(\varepsilon, \tau)$ as a function of carrier density ($n_2$) for given values of $\varepsilon$ and $\hbar/\tau$. It is found that $1/\tau^1_{ee}(\varepsilon, \tau)$ declines on increasing

$n_2$ for given values of $\varepsilon$ and $1/\tau$. However, this is to be seen, along with the fact that an increase in $n_2$ can be made at the expense of enhancing the disorder which in turn leads to shorter values of $\hbar/\tau$, in the case of a doped quantum well. Also, both the increase in $n_2$ and the enhancement in $\hbar/\tau$ affect the screened electron–electron interaction potential and the response function, $\xi_1(\boldsymbol{q}, \omega)$, which determines the value of $1/\tau^1_{ee}(\varepsilon, \tau)$ for a given value of $\varepsilon$. Our numerical computation of $1/\tau^1_{ee}(x, S)$ by choosing correct diffusive behaviour of $V_1(\boldsymbol{q}, \omega)$ and $\xi_1(\boldsymbol{q}, \omega)$, in the $q$–$\omega$ plane, suggests that a Fermi-liquid quasi-particle description is well justified for a 2D electron system with a random disorder potential.

## 4. 1D electron system (a quantum wire)

In the presence of a disorder potential, electrons in a degenerate system diffuse instead of moving ballistically. This plays an important role in determining several properties, such as transport properties. In the absence of a disorder potential, the Fermi surface of 1DEG smeared out and the momentum-space discontinuity in the distribution function disappears. Reconstruction of the Fermi surface takes place on introduction of a disorder potential in 1DEG. This suggests that, in the presence of randomized disorder potential, a Fermi-liquid quasi-particle description can be applied to the study of electron–electron scattering in 1DEG or in a QWR. The presence of disorder potential in a doped semiconductor device is unavoidable since a small amount of residual impurities is always there. This motivated us to calculate the electron–electron scattering rate, within the RPA, for a QWR consisting of a disorder potential. We consider a QWR along the $x$ axis with a $\delta$-function type confinement along the $z$ axis. We further assume that the electron wavefunction vanishes at the boundaries of the wire across the $y$ axis, at $y = \pm a/2$, where $a$ is the width of a QWR. The bare Coulomb potential between electrons in a QWR is given by [8]

$$V^0(q, y, y') = \frac{2e^2}{\varepsilon_0} k_0(q|y - y'|) \tag{18}$$

where $k_0(q|y - y'|)$ is the zeroth-order modified Bessel function. $q$ is the wavevector component along the $x$ axis. $k_0(q|y - y'|)$ can be taken as [29][1]

$$k_0(q|y - y'|) = \int_0^\infty \mathrm{d}t \, \frac{\exp\left(-|y - y'|\sqrt{t^2 + q^2}\right)}{\sqrt{t^2 + q^2}}. \tag{19}$$

$V^0(q)$, using equations (18) and (19), is then given by

$$V^0(q) = \frac{2e^2}{\varepsilon_0} \int_0^\infty \mathrm{d}t \, \frac{H(\lambda)}{\lambda}, \tag{20}$$

where

$$\lambda = \sqrt{t^2 + q^2}. \tag{21}$$

$H(\lambda)$ is the expectation value of $\exp(-\lambda|y - y'|)$. As mentioned before, we confine ourselves to the intrasubband electron–electron scattering within the ground subband. $H(\lambda)$ for intrasubband transitions is defined as [30]

$$H(\lambda) = \int_{-a/2}^{a/2} \mathrm{d}y \int_{-a/2}^{a/2} \mathrm{d}y' \, \exp(-\lambda|y - y'|)|\phi(y)|^2|\phi(y')|^2. \tag{22}$$

[1] The representation of the modified Bessel function 8.432 (9) for $\nu = 0$ reduces to equation (19). The $V^0(q, y, y')$ obtained using (18) and (19) will be used for $q > 0$ in subsequent descriptions.

Evaluation of equation (22) by taking $\phi(y)$ and $\phi(y')$ that vanish at $y = \pm a/2$ yields [30]

$$H(\lambda) = \left(\frac{u}{w} + \frac{2}{u}\right) - \frac{32\pi^4}{(wu)^2}(1 - \mathrm{e}^{-u}), \tag{23}$$

with $u = \lambda a$ and $w = u^2 + 4\pi^2$. For larger values of $a$ ($\gg 2\pi$), $H(u) \to 3/u$ and $V^0(q)$ reduces to $3\pi e^2/\varepsilon_0|qa|$ which agrees with the asymptotic forms of $V^0(q)$ reported in [8], whereas, for smaller values of $u$ ($\ll 1$), $H(u)$ goes to unity and equation (20) reduces to

$$V^0(q) = \frac{2e^2}{\varepsilon_0}\int_0^\infty \frac{\mathrm{d}t}{\sqrt{t^2 + q^2}}. \tag{24}$$

The $V^0(q)$ defined by equation (24) has been used to calculate $1/\tau_{\mathrm{ee}}(\varepsilon, \tau)$ for 1DEG [24]. The logarithmically divergent integral in equation (24) was cut-off by taking an upper limit, $q_c \sim 1/a$, to obtain $V^0(q)$ that well describes the interactions at distances much larger than $a$. The integrand in equation (20), compared to that in equation (24), has better convergence and it does not show logarithmic divergence at the upper limit, since $H(u) \to 0$ as $t \to \infty$. Also, equation (20) yields the correct $q$ and $a$ dependence of $V^0(q)$ and provides a better description of the bare Coulomb potential, as compared to that given by equation (24) for a QWR. The $\nu$ for intrasubband transitions within the ground state of a QWR is given by

$$\nu_2 = \frac{2m_{\mathrm{e}}^*}{\pi\hbar^2 k_{\mathrm{F}}}. \tag{25}$$

Evaluation of equation (6) with the use of (8) gives for a QWR

$$\xi_2(q, \omega) = \frac{\mathrm{i}}{\tau\varepsilon_{\mathrm{F}}}\frac{(\phi - \psi)}{[\phi\psi\{(\phi - \psi)^2 - (q/k_{\mathrm{F}})^2\}]}, \tag{26}$$

with

$$\phi = \sqrt{1 + \frac{\mathrm{i}}{2\tau\varepsilon_{\mathrm{F}}}} \tag{27}$$

$$\psi = \sqrt{1 - \frac{(\omega + \mathrm{i}/2\tau)}{\varepsilon_{\mathrm{F}}}}. \tag{28}$$

The $V_2(q, \omega)$ that has the correct diffusive behaviour for $\varepsilon \leqslant \varepsilon_{\mathrm{F}}$ is given by [8, 24]

$$V_2(q, \omega) = \frac{1}{\frac{\nu_2 D_2 q^2}{-\mathrm{i}\omega + D_2 q^2} + \frac{1}{V^0(q)}}, \tag{29}$$

where $0 \leqslant q \leqslant \omega/v_{\mathrm{F}}$. The $D_2 = v_{\mathrm{F}}^2\tau$ is the one-dimensional diffusion coefficient. Computation of equation (11) with the use of equations (20)–(29) yields the RPA value of $1/\tau_{\mathrm{ee}}^2(\varepsilon, \tau)$, which has been found to be unreasonably high for a realistic quantum wire. The previously reported RPA calculation of $1/\tau_{\mathrm{ee}}^2(\varepsilon, \tau)$, which has basically been performed for a larger value of $1/\tau(> \varepsilon)$, uses $q$- and $\omega$-independent $V_2(q, \omega)$ [24]. Also, the calculations based on the Tomonaga–Luttinger model have been performed by taking a screened electron–electron potential independent of both $q$ and $\omega$ [32, 33]. This motivated us to take static ($\omega$-independent) screened electron–electron interaction for computing $1/\tau_{\mathrm{ee}}^2(\varepsilon, \tau)$. As is seen from equation (30), use of a $\omega$-independent screened electron–electron potential is well justified when $\omega\tau \ll 1$. In the following we take

$$V_2(q, \omega) = \frac{1}{\nu_2 + 1/V^0(q)} \tag{30}$$

to compute the $1/\tau^2_{ee}(\varepsilon, \tau)$ for a realistic QWR. Equation (11) with the use of (25), (26) and (30) can be rewritten in terms of dimensionless quantities:

$$\frac{\hbar}{\tau^2_{ee}(x, S)\varepsilon_F} = \frac{1}{\pi}\int_0^x dy \int_0^{y/2} dz \, \frac{y}{[1+C(z)]^2}\left[\mathrm{Re}\left\{\frac{iB(y)}{A(y)(B^2(y)-z^2)-iSB(y)}\right\}\right]^2, \quad (31)$$

where $C(z) = \pi k_F \hbar^2/2m^* V^0(z)$, $A(y) = \sqrt{1+S^2/4-y(1+iS/2)}$ and $B(y) = \sqrt{1+iS/2} - \sqrt{1-y-iS/2}$.

The analytical solution of equation (31) with the use of equation (20) for all values of $x$ and $S$ up to unity is not possible. A closer look at equations (20) and (31) suggests that $z$ values close to the lower limit ($z = 0$) make the maximum contribution to $z$ integration. For these values of $z$, $V^0(z)$ tends to a very large value, since it diverges for $z \to 0$. This suggests that, to retain the major contributions to $\hbar/\tau^2_{ee}(x, S)\varepsilon_F$ from $z$ and $y$ integrations, we can take $V_2(q, \omega) \approx 1/\nu_2$, $A \cong 1$ and $B \cong (y + iS)/2$, which is justified for $x \ll 1$ and $S \ll 1$. Equation (31) then simplifies to

$$\frac{\hbar}{\tau^2_{ee}(x, S)\varepsilon_F} = \frac{4S^2}{\pi}\int_0^x y\, dy \int_0^{y/2} \frac{dz}{(y^2+S^2-4z^2)^2}. \quad (32)$$

The evaluation of $z$ and $y$ integrations yields

$$\frac{\hbar}{\tau^2_{ee}(x, S)\varepsilon_F} = \frac{x}{\pi} + \frac{S^2}{2\pi\sqrt{S^2+x^2}} \ln\left[\frac{\sqrt{S^2+x^2}-x}{\sqrt{S^2+x^2}+x}\right]. \quad (33)$$

We have used: (i) the screened electron–electron interaction potential and (ii) a linear wavevector-dependent energy difference between two electronic states in obtaining equations (32) and (33). The calculations that are based on the Tomonaga–Luttinger model [31, 32] have also been performed using a constant screened electron–electron potential and linear wavevector-dependent energy eigenvalues. Therefore, our approach of obtaining analytical results given by equation (33) is similar to the treatment within the Tomonaga–Luttinger model [31, 32]. The simple solvable model for zero-range potentials, which are analogous to our treatment, can be found elsewhere [33].

We computed $\hbar/\tau^2_{ee}(x, S)\varepsilon_F$ for a GaAs quantum wire that has $m^*_e = 0.068\ m_e$ and $\varepsilon_0 = 12.5$. Our numerically computed results using equations (31) and (20) along with $\hbar/\tau^2_{ee}(x, S)\varepsilon_F$ from equation (33) are plotted as a function of normalized energy in figure 4, for $k_F = 10^6$ cm$^{-1}$, two values of normalized broadening (0.1 and 0.4) and two values of the width of the quantum wire (20 and 50 Å). The figure shows that agreement between the analytical and numerically computed results is very good when $x \ll 1$ and it is fairly good for the rest of the values of $x$. As is seen from the figure, the magnitude as well as the $x$ dependence of $\hbar/\tau^2_{ee}(x, S)\varepsilon_F$ change, more obviously at larger values of $x(>0.2)$ and smaller values of $S(<0.2)$, on replacing the $q$-independent screened electron–electron potential by a $q$-dependent one. Previously reported approximate calculations show that the $\hbar/\tau^2_{ee}(x, S)\varepsilon_F$ is proportional to $\sqrt{x}$ at smaller values of $x$ when $S$ is large ($\sim$ unity) [24]. In support of earlier findings, our computed curves D and E also exhibit $\sqrt{x}$-dependent type behaviour, as is seen from the figure. We further find that the computed curve E can almost be fitted to $\hbar/\tau^2_{ee}(x, S)\varepsilon_F = \alpha\sqrt{x} + \beta x$, where $\alpha$ and $\beta$ depend on $h/\tau$ and $k_F$. The magnitude of $\hbar/\tau^2_{ee}(x, S)\varepsilon_F$ has been found to be decreasing on increasing $a$, for all values of $x$ and $S$. Our computed $\hbar/\tau^2_{ee}(x, S)\varepsilon_F$ as a function of the wire width, using equations (31) and (20), for $x = 0.4$, $S = 0.1$ and $k_F = 10^6$ cm$^{-1}$ is displayed in figure 5. The $\hbar/\tau^2_{ee}(x, S)\varepsilon_F$ tends to $\hbar/\tau^1_{ee}(x, S)\varepsilon_F$ for larger values of the wire width, as is seen from figures 2 and 5. Figure 5 suggests that the electron–electron scattering becomes stronger on decreasing the width of a QWR, when other intrinsic parameters are kept unchanged.

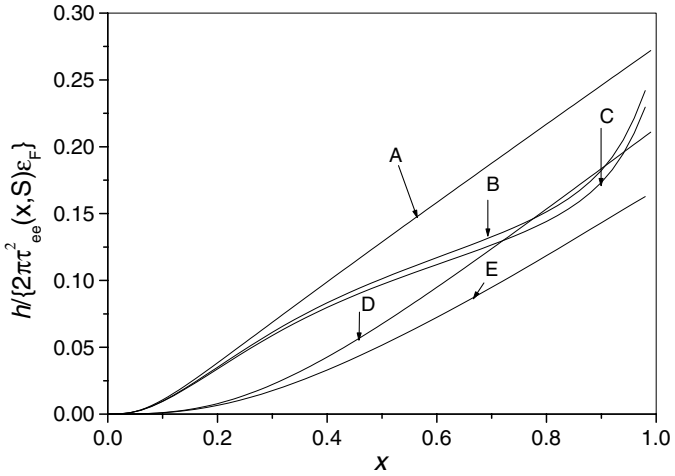


**Figure 4.** Dimensionless electron–electron scattering rate as a function of normalized energy for a quantum wire at $\varepsilon_F = 5.6$ meV, $\varepsilon_0 = 12.5$ and $k_F = 10^6$ cm$^{-1}$. Analytical results from equation (33): curve A, when $a = 50$ Å and $\hbar/\tau\varepsilon_F = 0.1$; curve D, when $a = 50$ Å and $\hbar/\tau\varepsilon_F = 0.4$. Numerically computed results from equation (31): curve B, for $a = 20$ Å and $\hbar/\tau\varepsilon_F = 0.1$; curve C, when $a = 50$ Å and $\hbar/\tau\varepsilon_F = 0.1$; curve E, for $a = 50$ Å and $\hbar/\tau\varepsilon_F = 0.4$.

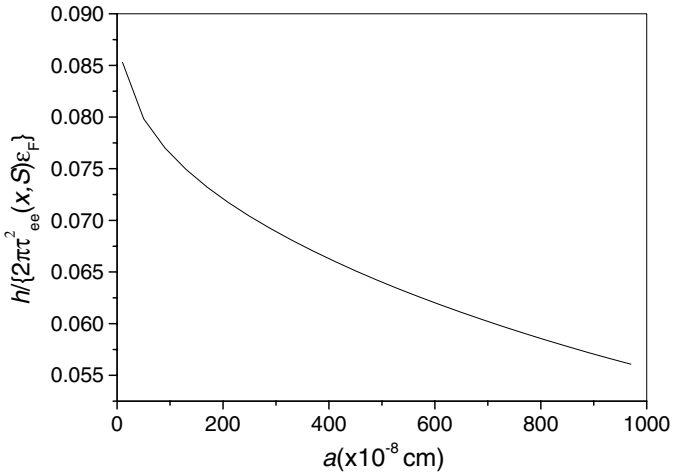


**Figure 5.** Dimensionless electron–electron scattering rate of a quantum wire as a function of wire width when $\varepsilon_0 = 12.5$, $k_F = 10^6$ cm$^{-1}$, $\varepsilon_F = 5.6$ meV, $\varepsilon/\varepsilon_F = 0.4$ and $\hbar/\tau\varepsilon_F = 0.1$.

We have also computed $\hbar/\tau_{ee}^2(x, S)\varepsilon_F$, using equations (31) and (20), as a function of $k_F$ for $\varepsilon = 2.24$ meV, $a = 50$ Å and $\hbar/\tau = 0.56$ meV. Our computed results show that the electron–electron scattering rate is enhanced on decreasing the carrier density, when $\hbar/\tau$, $\varepsilon$ and the width of the wire are kept constant. However, in a doped quantum wire, an increase in carrier density can only be made at the cost of increased disorder and thermalization, which is not considered in computing $\hbar/\tau_{ee}^2(x, S)\varepsilon_F$ as a function of carrier density.

To understand further the role of electron-disorder potential scattering in electron–electron scattering in a quantum wire, we computed $\hbar/\tau_{ee}^2(x, S)\varepsilon_F$ as a function of $S$ for given values of $x$, $a$ and $k_F$. Our numerically computed results from equations (31) and (20) along with

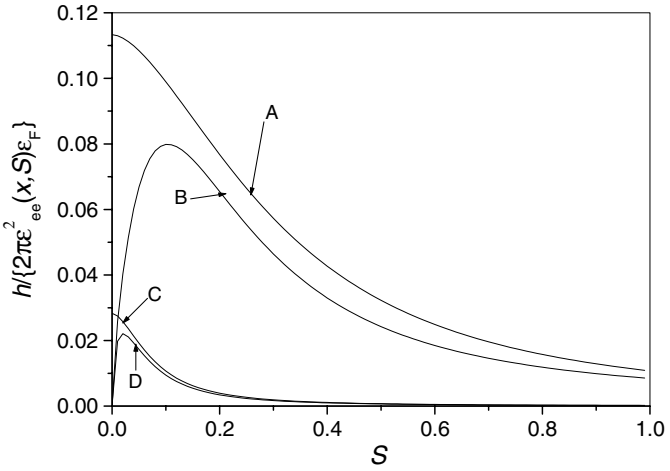


**Figure 6.** Dimensionless electron–electron scattering rate as a function of normalized broadening for a quantum wire at $\varepsilon_F = 5.6$ meV, $\varepsilon_0 = 12.5$ and $k_F = 10^6$ cm$^{-1}$. Analytical results from equation (33): curve A, when $a = 50$ Å and $\varepsilon/\varepsilon_F = 0.4$; curve C, when $a = 50$ Å and $\varepsilon/\varepsilon_F = 0.1$. Numerically computed results from equation (31): curve B, for $a = 50$ Å and $\varepsilon/\varepsilon_F = 0.4$; curve D, when $a = 50$ Å and $\varepsilon/\varepsilon_F = 0.1$.

those from equation (33) are displayed in figure 6 for two values of normalized energy (0.1 and 0.4), $a = 50$ Å and $k_F = 10^6$ cm$^{-1}$. As is expected, equation (33) shows very good agreement with numerically computed results from equations (31) and (20), when $x \ll 1$. The agreement between simple analytical results and the detailed numerical results is good even at higher values of $S$ and $x$. It has to be noted that, for smaller values of $S(<0.1)$, numerically computed $\hbar/\tau_{ee}^2(x, S)\varepsilon_F$ from equations (31) and (20) decline on decreasing $S$. However, the range of $S$ values for which $\hbar/\tau_{ee}^2(x, S)\varepsilon_F$ increases on increasing $S$ narrows down on reducing $x$, as is seen from the figure. Equation (33) does not exhibit this kind of behaviour. In our opinion, the decline in $\hbar/\tau_{ee}^2(x, S)\varepsilon_F$ on decreasing $S$ $(<0.1)$ does not relate to any new physical phenomenon but probably it is the regime of $x$ and $S$ where RPA fails to provide a satisfactory description of electron–electron scattering in a quantum wire. The assumptions made to obtain $\xi_2(q, \omega)$ may not remain valid for these values of $x$ and $S$. Nevertheless, the results presented in this section suggest that electron–electron scattering in the presence of a significant disorder potential can be very well described within a Fermi-liquid treatment by taking into account the correct diffusive behaviour of the electron gas in a quantum wire.

## 5. Quantum wire system

A 1D periodic sequence of quantum wires is known as a QWS. A quantum wire consists of a strong epitaxial confinement along one direction and a weak confinement along another direction. We take a delta function type confinement along the $z$ axis and an infinite potential well type confinement along the $y$ axis for a quantum wire. A typical quantum wire structure is depicted in figure 7, where the width of a wire along the $z$ axis is negligibly small. The bare Coulomb potential for electrons in a QWS can be given by [34]

$$V^0(q, q') = \frac{2e^2}{\varepsilon_0} \sum_{l=l'} \int \int k_0(q|(l-l')d + (y-y')|) \times \exp\{-\mathrm{i}q'(l-l')d\}|\phi(y)|^2|\phi(y')|^2 \,\mathrm{d}y\,\mathrm{d}y', \tag{34}$$

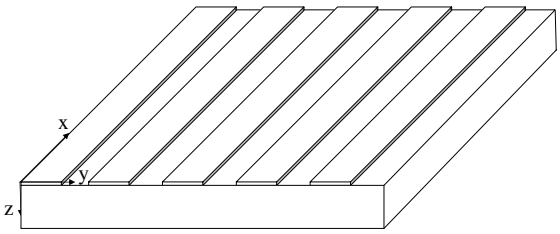


**Figure 7.** A typical quantum wire structure used to calculate electron–electron interaction.

where $q$ and $q'$ are the wavevector components along the $x$ axis and $y$ axis, respectively. The $l$ and $l'$ are the quantum wire indices. The Bessel function $k_0(|q(l-l')d+(y-y')|)$ can be represented in several ways. Li and Das Sarma evaluated $V^0(q,q')$ using a periodic boundary condition along the $y$ axis on assigning a finite size to the QWS [32]. However, their results do not yield correct limiting values of $V^0(q,q')$ for $d \to 0$ and $\infty$. One of the forms of $k_0\{q(y-y')\}$ that yields the correct limiting values of $V^0(q,q')$ is given by equation (19). We solve equation (34) using equation (19) to get [30]

$$V^0(q,q') = \frac{2e^2}{\varepsilon_0}\int_0^\infty \frac{U(\lambda,q')}{\lambda}\,\mathrm{d}t \tag{35}$$

with

$$U(\lambda,q') = H(\lambda) - C(\lambda)[1-S(\lambda,q')]. \tag{36}$$

$\lambda$ defined by equation (21) and $C(\lambda)$ is given by equation (22) on replacing $\exp(-q|(t-t')|)$ by $\exp\{-q'(t-t')\}$. Evaluation of $S(\lambda,q')$ and $C(\lambda)$ gives [30]

$$S(\lambda,q') = \frac{\sinh(\lambda d)}{\cosh(\lambda d)-\cos(q'd)} \tag{37}$$

$$C(\lambda) = \frac{16\pi^4}{(uw)^2}(1-\mathrm{e}^{-u})(1-\mathrm{e}^{u}). \tag{38}$$

$H(\lambda)$, $u$ and $w$ are defined earlier in section 4. Equation (35) reduces to (20) for $d \to \infty$, while for $d \to 0$ it describes the bare Coulomb potential of a QWL. Following the arguments presented in section 4, the screened Coulomb interaction between electrons for a QWR, in the diffusive regime, is given by

$$V_3(q,q') = \frac{1}{\nu_2 + 1/V^0(q,q')} \tag{39}$$

where $q'$ varies over a unit cell of width $d$ along the $y$ axis and it takes discrete values restricted by $-\pi/d \leqslant q' \leqslant \pi/d$. $\hbar/\tau_{\mathrm{ee}}^3(x,S)$ in terms of dimensionless quantities is given by

$$\frac{\hbar}{\tau_{\mathrm{ee}}^3(x,S)\varepsilon_{\mathrm{F}}} = \frac{k_{\mathrm{F}}d}{2\pi^2}\int_0^x \mathrm{d}y \int_0^{y/2}\mathrm{d}z\int_{-\varphi}^{\varphi}\mathrm{d}z'\frac{y}{[1+C(z,z')]^2} \times\left[\mathrm{Re}\left\{\frac{\mathrm{i}B(y)}{A(y)(B^2(y)-z^2)-\mathrm{i}SB(y)}\right\}\right]^2, \tag{40}$$

where $\varphi = \pi/k_{\mathrm{F}}d$, $z' = q'/k_{\mathrm{F}}$ and $C(z,z') = \pi k_{\mathrm{F}}\hbar^2/2m^*V^0(z,z')$.

An analytical solution of equation (40) is not possible. The behaviour of $V^0(z,z')$ with $z$ after integration over $z'$ is found to be very similar to that of $V^0(z)$ for a QWR. This suggests that a naive analytical solution of equation (40) can be given by equation (33). We computed equation (40) numerically for a GaAs/$\mathrm{Al}_x\mathrm{Ga}_{1-x}$As QWS system by modelling it as a 2D

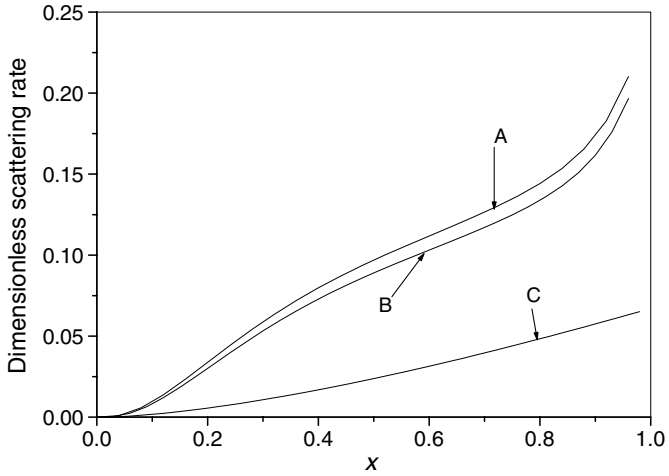


**Figure 8.** Numerically computed electron–electron scattering rate as a function of normalized energy for $\varepsilon_0 = 12.5$. Curve A is for a quantum wire from equation (31) at $\varepsilon_F = 5.6$ meV, $a = 50$ Å, $k_F = 10^6$ cm$^{-1}$ and $\hbar/\tau\varepsilon_F = 0.1$. Curve B is for a quantum wire system from equation (40) for $\varepsilon_F = 5.6$ meV, $a = 50$ Å, $d = 125$ Å, $k_F = 10^6$ cm$^{-1}$ and $\hbar/\tau\varepsilon_F = 0.1$. Curve C is for a quantum well from equation (14) at $k_F = 3.45 \times 10^6$ cm$^{-1}$ and $\varepsilon_F = 35.25$ meV.

periodic sequence of 1D wires embedded in a dielectric medium with an average dielectric constant, $\varepsilon_0 = 12.5$. For computation of our results, we took $a = 5$ nm, $d = 12.5$ nm and $k_F = 10^6$ cm$^{-1}$. Our numerically computed $\hbar/\tau^3_{ee}(x, S)$ along with $\hbar/\tau^2_{ee}(x, S)$ from equation (31) and $\hbar/\tau^1_{ee}(x, S)$ from equation (14) are plotted in figure 8, as a function of normalized energy for $S = 0.1$. The figure shows that $\hbar/\tau^3_{ee}(x, S)$ is smaller than $\hbar/\tau^2_{ee}(x, S)$ and it is larger than $\hbar/\tau^1_{ee}(x, S)$, for all values of $x$. However, the nature of the $\hbar/\tau^3_{ee}(x, S)$ versus $x$ curve is similar to that of the $\hbar/\tau^2_{ee}(x, S)$ versus $x$ curve. Both intra-wire and inter-wire electron–electron interactions contribute to $\hbar/\tau^3_{ee}(x, S)$, whereas $\hbar/\tau^2_{ee}(x, S)$ is contributed by intra-wire interactions only. The major contribution to $\hbar/\tau^3_{ee}(x, S)$, however, come from intra-wire interactions if the separation between two consecutive wires is larger than the width of a wire. This can very well be seen from the figure when $d > a$. An important result that emerges from the figure is the enhancement of the electron–electron scattering rate on reducing the effective dimensionality of the system.

## 6. Discussions and conclusion

We computed $1/\tau^1_{ee}(\varepsilon, \tau)$, $1/\tau^2_{ee}(\varepsilon, \tau)$ and $1/\tau^3_{ee}(\varepsilon, \tau)$ by taking the correct diffusive behaviour of a screened electron–electron interaction potential and the response function $\xi(q, \omega)$ in the $q$–$\omega$ plane for zero temperature. The magnitude and the $\varepsilon$ dependence of $1/\tau^1_{ee}(\varepsilon, \tau)$, $1/\tau^2_{ee}(\varepsilon, \tau)$ and $1/\tau^3_{ee}(\varepsilon, \tau)$ is determined by the values of the intrinsic parameters $\hbar/\tau$, $k_F$ and $a$. The numerically computed values of $1/\tau^1_{ee}(\varepsilon, \tau)$ as a function $\varepsilon$ can almost be fitted to a polynomial of type $1/\tau^1_{ee}(\varepsilon, \tau) = a\varepsilon + b\varepsilon^2 + c\varepsilon^3$ for $0 \leqslant \varepsilon \leqslant \varepsilon_F$. The $1/\tau^1_{ee}(\varepsilon, \tau)$, $1/\tau^2_{ee}(\varepsilon, \tau)$ and $1/\tau^3_{ee}(\varepsilon, \tau)$ exhibit the largest value for $\hbar/\tau \to 0$ and they decline monotonically on increasing $\hbar/\tau$ for given values of $\varepsilon, a$ and $k_F$. The presence of disorder weakens the electron–electron scattering rate. A small amount of residual impurities is unavoidable and therefore electron-disorder potential scattering cannot completely be ignored in a doped semiconductor nanostructure. As is expected, the computed $1/\tau^2_{ee}(\varepsilon, \tau)$ declines

with $a$ and it tends to $1/\tau_{ee}^{1}(\varepsilon,\tau)$ for large values of $a$ ($>$50 nm), when $\hbar/\tau$, $\varepsilon$ and $k_F$ are kept unchanged. The $1/\tau_{ee}^{2}(\varepsilon,\tau)$ varies as $\sqrt{\varepsilon}$ for smaller values of $\varepsilon$ and as a linear function of $\varepsilon$ at larger values ($\sim\varepsilon_F$), when $\hbar/\tau$ is of the order of unity. It is found that $1/\tau_{ee}^{1}(\varepsilon,\tau) < 1/\tau_{ee}^{2}(\varepsilon,\tau) > 1/\tau_{ee}^{3}(\varepsilon,\tau)$, for given values of $\varepsilon$, $\hbar/\tau$, $a$ and $k_F$. The inter-wire electron–electron interactions, which are absent in a quantum wire, weaken the electron–electron scattering. Both intra-wire and inter-wire interactions contribute to the electron–electron scattering rate in the case of a quantum wire structure. The electron gas in a QWS exhibits the quasi-1D behaviour and the screened electron–electron interaction potential is weaker in a QWS compared to that in a QWR. We thus find that the electron–electron scattering rate enhances on reducing the effective dimensionality of a system. The simple analytical results given by equations (14) and (33) provide the reasonably good description of the electron–electron scattering rate, in the presence of disorder, for a quantum well and a quantum wire, respectively, especially when $\varepsilon$ and $\hbar/\tau$ are much smaller than the Fermi energy. Our theoretical study of $1/\tau_{ee}^{1}(\varepsilon,\tau)$, $1/\tau_{ee}^{2}(\varepsilon,\tau)$ and $1/\tau_{ee}^{3}(\varepsilon,\tau)$, within the RPA framework, suggests that a Fermi-liquid quasi-particle description can be applied to electron–electron scattering, in the presence of a disorder potential, in a QWL, QWR and QWS. Also, a theoretical description of electron–electron scattering in the presence of electron–impurity scattering is possible beyond the Tomonaga–Luttinger model for low dimensional systems. The results presented in this paper can be used to estimate quantum corrections to conductivity, the damping of collective excitations and the optical properties of nanostructures.

## Acknowledgment

The authors acknowledge the financial support from the Department of Science and Technology, Government of India, in carrying out this work.

## References

[1] Jungwirth T and Macdonald A H 1996 *Phys. Rev.* B **53** 7403
[2] Fukuyama H and Abrahams E 1983 *Phys. Rev.* B **27** 5976
[3] Reizer M and Wilkins J W 1997 *Phys. Rev.* B **55** R7363
[4] Abrahams E, Anderson P W, Lee P A and Ramakrishnan T V 1981 *Phys. Rev.* B **24** 6783
[5] Giuliani G F and Quinn J J 1982 *Phys. Rev.* B **26** 4421
[6] Zheng L and Das Sarma S 1996 *Phys. Rev.* B **53** 9961
[7] Thakur J S and Neilson D 1997 *Phys. Rev.* B **56** 4679
[8] Hu B Y-K and Das Sarma S 1993 *Phys. Rev.* B **48** 5469
[9] Ramsak A, Rejee T and Jefferson J H 1995 *Phys. Rev.* B **58** 4014
[10] Brouwer P W, Mudry C and Furusaki A 2001 *Physica* E **9** 333
[11] Sablikov V A and Shchamkhalova B S 1998 *Phys. Rev.* B **58** 13847
[12] Das Sarma S and Hwang E H 1996 *Phys. Rev.* B **54** 1936
[13] Lee P A and Ramakrishnan T V 1985 *Rev. Mod. Phys.* **57** 287
[14] Echenique P M, Pitarke J M, Churkov E V and Rubio A 2000 *Chem. Phys.* **251** 1
[15] Sharma A C and Tripathi P 2000 *Physica* E **8** 306
[16] Predel H, Buhmann H, Molenkump L W, Gurzhi R N, Kalineiko A N, Kopeliovich A T and Yanovsky A V 2000 *Phys. Rev.* B **62** 2057
[17] Nagy I, Alducin M, Juaristio J I and Echenique P M 2001 *Phys. Rev.* B **64** 075101
[18] Lin J J, Xu W, Zheng Y L, Huang J H and Huang Y S 1999 *Phys. Rev.* B **59** 344
[19] Hu B Y-K and Flensberg K 1996 *Phys. Rev.* B **53** 10072
[20] Maurov H and Giamarchi T 1995 *Phys. Rev.* B **51** 10833
[21] Fasol G and Sakaki H 1993 *Phys. Rev. Lett.* **70** 3643
[22] Tavares M R S, Das Sarma S and Hai G-Q 2000 *Preprint* cond-mat/0004056 v1
[23] Lewalle A, Pepper M, Ford C J B, Hwang E H, Das Sarma S, Paul D J and Redmond G 2002 *Physica* E **12** 616

[24] Altshuler B L, Aronov A G, Khnelnitskii D E and Larkin A I 1982 *Quantum Theory of Solids* ed I M Lifshits (Moscow: Mir) p 1553
[25] See e.g., Richter K 1999 *Semiclassical Theory of Mesoscopic Quantum Systems* (New York: Springer) p 138
[26] Nixon J A and Davies J H 1990 *Phys. Rev.* B **41** 7929
[27] Gold A, Allen S J, Wilson B A and Tsui D C 1982 *Phys. Rev.* B **25** 3519
[28] Sharma A C and Sen R 1995 *J. Phys.: Condens. Matter* **7** 9551
[29] See, for example, Gradshteyn I S and Ryzhik I M *Table of Integrals Series and Products* ed A Jeffrey (New York: Academic) p 969
[30] Sharma A C and Bajpai A 2002 *Int. J. Mod. Phys.* B **16** 1511
[31] Dzyaloshinskii I E and Larkin A I 1973 *Zh. Eksp. Teor. Phys.* **65** 411
[32] See, e.g., Mahan G D 1990 *Many Particle Physics* 2nd edn (New York: Plenum)
[33] See for example, Albeverio S, Hoegh-Krohn R, Gesztesy F and Holden H 1988 *Solvable Models in Quantum Mechanics* (New York: Springer)
[34] Li Q P and Das Sarma S 1996 *Phys. Rev.* B **43** 11768